Title: Idiosyncratic and dose-dependent epistasis drives variation in tomato fruit size

Authors: Lyndsey Aguirre[1], Anat Hendelman[2], Samuel F. Hutton[3], David M. McCandlish[2*], Zachary B. Lippman[1,2,4*]

Affiliations:
[1]Cold Spring Harbor Laboratory, School of Biological Sciences, Cold Spring Harbor, NY, USA.
[2]Cold Spring Harbor Laboratory; Cold Spring Harbor, NY, USA.
[3]Gulf Coast Research and Education Center, University of Florida, Wimauma, FL, USA.
[4]Howard Hughes Medical Institute, Cold Spring Harbor Laboratory, Cold Spring Harbor, NY, USA.
[*]Corresponding authors. Email: mccandlish@cshl.edu, lippman@cshl.edu

Abstract: Epistasis between genes is traditionally studied using mutations that eliminate protein activity, but most natural genetic variation is in cis-regulatory DNA and influences gene expression and function quantitatively. Here, we use natural and engineered cis-regulatory alleles in a plant stem cell circuit to systematically evaluate epistatic relationships controlling tomato fruit size. Combining a promoter allelic series with two other loci, we collected over 30,000 phenotypic data points from 46 genotypes to quantify how allele strength transforms epistasis. We revealed a saturating dose-dependent relationship, but also allele-specific idiosyncratic interactions, including between alleles driving a step change in fruit size during domestication. Our approach and findings expose an underexplored dimension of epistasis, where cis-regulatory allelic diversity within gene regulatory networks elicits non-linear, unpredictable interactions that shape phenotypes.

One-Sentence Summary: Epistasis analysis across a cis-regulatory allelic series reveals unpredictable, non-linear interactions that shape trait variation.

Main Text: Epistasis analysis is an essential tool for discovering functional relationships between genes. At its simplest, an epistatic interaction is determined by testing if the phenotypic effect from one gene mutation modifies (e.g. suppresses or enhances) the phenotypic effect of another (*1*, *2*). Historically, epistasis studies have relied on mutations with strong effects on protein function and phenotype, typically obtained from natural mutants or laboratory mutagenesis experiments (*1–4*). Recently, high-throughput engineering and the combination of gene deletions in yeast have allowed for the characterization of global interaction networks (*5–10*). While these and related studies, including those now leveraging genome-editing technologies in more complex systems (*11–15*), can dissect epistasis at scale, they do not address how cis-regulatory mutations, which are pervasive in genomes and responsible for the majority of functional variation in organisms (*16–19*), impact epistatic relationships and the phenotypes they control.

Compared to protein-coding mutations, cis-regulatory mutations more often produce graduated effects on gene function that alter expression level or timing (*16*, *20*, *21*). Across species, natural variation in gene expression is predominantly associated with regulatory sequences of the differentially expressed genes (*16*, *19*, *22*), and cis-regulatory variants are the primary contributors to phenotypic diversity (*16*, *18*). Despite their critical functional role, few studies have explored epistatic relationships in the context of cis-regulatory variation (*5*, *10*, *23*), and none have done so in depth. Due to limited allelic variation at known interacting genes and inadequate quantitative phenotyping power in most model systems, we lack an understanding of how this widespread genetic variation affects the form and magnitude of epistasis.

We addressed this knowledge gap by taking advantage of the *CLAVATA-WUSCHEL* (*CLV-WUS*) gene regulatory circuit in plants (*24*). *CLV-WUS* controls stem cell proliferation in small groups of cells at shoot apices called meristems, which enable the continuous development of new tissues and organs during post-embryonic growth (*24*). Using tomato as a model, we asked how previously documented epistatic interactions in this circuit are affected by replacing one critical gene, *CLAVATA3* (*CLV3*), with a wide range of stronger and weaker cis-regulatory alleles.

CLV3 encodes a small signaling peptide that restricts stem cell proliferation and meristem size by repressing *WUS*, a stem-cell-promoting homeobox transcription factor gene (*24*). In a negative feedback loop, *WUS* suppresses its own expression by activating *CLV3* to restrict stem cell proliferation and maintain meristem size throughout development (*24*). Epistasis between *CLV3* and *WUS* was first established using mutants in the model *Arabidopsis thaliana* (*25*), and our previous CRISPR-Cas9 mutagenesis of the tomato orthologues has shown this relationship is conserved (*26–28*). In both systems, meristem growth in *wus* mutants ceases during vegetative development, resulting in a failure to develop flowers and fruits. Conversely, meristems of *clv3* mutants become greatly enlarged, leading to more flowers, fruits, and their associated organs, including seed compartments known as locules. In a classical suppression epistatic relationship, *wus* mutations completely mask *clv3* phenotypes (i.e. *clv3 wus* double mutants are indistinguishable from *wus* single mutants). Tomato also features an additional layer of epistasis involving a paralog of *SlCLV3* (*Solanum lycopersicum*, denoted by '*Sl*') in the *CLV3/EMBRYO-SURROUNDING REGION* (*CLE*) gene family, *SlCLE9* (*27*). *SlCLE9* is an ancient paralog, whose natural allelic state in wild and domesticated tomatoes is a partial loss-of-function (i.e. hypomorphic) due to changes in both its protein sequence and cis-regulatory control (*27*, *29*). While null mutants of *Slcle9* are indistinguishable from wild-type plants, *Slclv3* is strongly enhanced by *Slcle9*, demonstrating a canonical unequal redundancy (*30*) epistatic relationship between these paralogs.

Although conventional protein-coding null mutations were used to characterize these epistatic relationships, two natural cis-regulatory alleles of *SlWUS* and *SlCLV3,* are also known to exhibit a strong epistatic interaction (*26*) . In fact, this interaction played an important role in

the expansion of fruit size via an increase in locule number that occurred during tomato domestication (*26*, *31*). Specifically, the ancestral state of tomato, which is maintained in many cultivated genotypes, is to produce fruits with two or three locules (Fig. 1A). A quantitative trait locus (QTL) allele known as *locule number* (*lc*) then emerged in the progenitor of modern tomatoes (*31*). This allele disrupts a repressor element downstream of *SlWUS* ($Slwus^{lc}$), leading to a weak gain-of-function and a slight increase of approximately 10% in the number of three-locule fruits (*26*). Subsequently, another QTL allele, *fasciated* (*fas*), arose in the form of an inversion that reduces the activity of the *SlCLV3* promoter ($Slclv3^{fas}$) (*26*, *31*), resulting in twice as many locules compared to wild-type (WT, $SlCLV3^{FAS}$). The combination of these cis-regulatory alleles in homozygous double mutant plants ($Slclv3^{fas}$ $Slwus^{lc}$) produces an enhanced (i.e. synergistic) epistatic effect on locule number that surpasses their combined individual effects (Fig. 1A) (*26*). Thus, the emergence of $Slclv3^{fas}$ in the context of the pre-existing $Slwus^{lc}$ background is thought to have been a key step in the increase in fruit size observed during tomato domestication (*31*). However, additional cis-regulatory alleles of the *SlCLV3* locus exist (*32*, *33*), and it remains an open question whether this synergistic interaction is specific to $Slclv3^{fas}$ or whether other cis-regulatory alleles of this gene with varying allelic strengths would also exhibit epistatic enhancement with $Slwus^{lc}$.

Epistasis across an allelic series of cis-**regulatory mutations**

Using natural alleles to investigate the impact of cis-regulatory allelic diversity on epistatic interactions in any system is challenging, due to their varied genetic backgrounds and limited understanding of their phenotypic effects. Previously, we used CRISPR/Cas9 to engineer cis-regulatory deletion mutations that overlapped with the disrupted cis-regulatory sequences of $Slwus^{lc}$ and $Slclv3^{fas}$, resulting in mimics of their individual effects in the same genetic background (*26*, *28*). In the same experiment, we engineered an additional 28 *Slclv3* promoter alleles ($Slclv3^{Pro}$), resulting in a continuum of locule number variation from subtle increases in the proportion of three-locule fruit to strong *Slclv3* null-like effects, shown in fruits that on average contain more than 15 locules (*28*). Leveraging this genetic resource, and its power to quantify locule number over a wide phenotypic range, we tested whether the $Slwus^{lc}$ mimic ($Slwus^{CR\text{-}lc}$) consistently enhances the effects of $Slclv3^{Pro}$ cis-regulatory alleles to the same degree as with $Slclv3^{fas}$ or whether epistatic interactions are dependent on the allelic strength and/or specific identity of the $Slclv3^{Pro}$ alleles.

From the pool of available $Slclv3^{Pro}$ alleles, we selected 12 that represent the full spectrum of locule number variation, including $Slclv3^{fas}$, and demonstrated that their homozygous mutant effects are reproducible across multiple years and environments (fig. S1A and table S3). This resource allowed us to measure how the magnitude of the epistatic interaction with $Slwus^{CR\text{-}lc}$ changes across this allelic series of cis-regulatory mutants (Fig. 1C). To evaluate the combined effects of $Slclv3^{Pro}$ and $Slwus^{CR\text{-}lc}$ cis-regulatory alleles, we created all possible double mutant combinations in the same genetic background as the single mutants (Fig. 1B and fig. S1A-B). We then quantified locule numbers from all $2 \times 12 = 24$ genotypes, including WT and single mutants, across two replicated experiments (Fig. 1B-C and fig. S2A).

We considered several specific hypotheses on how the magnitude of this epistatic interaction (table S2) might change as a function of cis-regulatory allelic strength: the absence of epistasis from $Slwus^{CR\text{-}lc}$ (i.e. additivity), and three modes of epistasis across the $Slclv3^{Pro}$ allelic series: proportional, constant, and idiosyncratic (Fig. 1D). In proportional epistasis (also known as the multilinear model) (*34*), the $Slwus^{CR\text{-}lc}$ effect scales linearly with $Slclv3^{Pro}$ allelic strength, whereas in constant epistasis the $Slwus^{CR\text{-}lc}$ effect is the same for each mutant allele. Idiosyncratic

epistasis, on the other hand, is allele-specific in that the *Slwus*$^{CR\text{-}lc}$ effect varies, potentially in either positive or negative directions, depending on the *Slclv3*^{Pro} mutant background (*35*, *36*).

To test these hypotheses, we built a nested family of models and fit them to the log-transformed data using maximum likelihood (Supplementary Materials). This analysis found that although neither the constant nor proportional epistasis models provided a better fit than the additive model (likelihood ratio test, p=.88 and p=.32, respectively), the additive, constant epistasis, and proportional epistasis models could all be rejected in favor of the idiosyncratic epistasis model (likelihood ratio test, p<.0001 against all simpler models). Thus, the effect of *Slwus*$^{CR\text{-}lc}$ across the *Slclv3*^{Pro} allelic series is neither constant nor a simple function of allelic strength but rather varies substantially in an allele-specific manner (Fig. 1E). A notable example is *Slclv3*$^{Pro\text{-}22}$. While this single mutant displays higher locule numbers than both the *Slclv3*^{fas} and *Slclv3*^{fas} *Slwus*$^{CR\text{-}lc}$ genotypes, counter to expectations, in the background of *Slclv3*$^{Pro\text{-}22}$, *Slwus*$^{CR\text{-}lc}$ actually decreases locule number, constituting a strong negative idiosyncratic effect (Fig. 1C-E). Moreover, our analysis also shows that the strong positive idiosyncratic effect from *Slwus*^{lc} on the *Slclv3*^{fas} background was not observed with any other *Slclv3*^{Pro} alleles (Fig. 1E). Thus, the combined effect on locule number from *Slclv3*^{fas} and *Slwus*^{lc} played a unique and critical role in enhancing fruit size during domestication, beyond what their individual effects could achieve.

The idiosyncratic epistasis between *Slwus*$^{CR\text{-}lc}$ and a subset of specific *Slclv3*^{Pro} alleles was surprising given the continuous phenotypic variation produced across the *Slclv3*^{Pro} allelic series. This raised the question of whether such unpredictability would be recapitulated with mutations of *SlCLE9,* which enhance the effects of both the *Slclv3* null mutation and the *Slclv3*^{fas} cis-regulatory mutation (*27*). Notably, similar to *Slclv3* null alleles, the expression of *SlCLE9* is upregulated in *Slclv3*^{fas} mutant meristems, though to a lesser degree (*27*). We confirmed this result and further showed that, overall, across the *Slclv3*^{Pro} allelic series, *SlCLE9* expression increases as *SlCLV3* expression decreases (fig. S3) as one moves from low to high locule number alleles. These observations suggested that, unlike the idiosyncratic epistasis imposed by *Slwus*$^{CR\text{-}lc}$ on the *Slclv3*^{Pro} allelic series, *Slcle9* could progressively enhance locule numbers across the allelic series, which would support proportional epistasis (Fig. 1D).

Utilizing the same *Slclv3*^{Pro} mutants and approach as for *Slwus*$^{CR\text{-}lc}$ (Fig. 2A and fig. S1C), we unexpectedly found that for *Slcle9* all of the simpler models were again rejected in favor of the idiosyncratic epistasis model (likelihood ratio test, p<.0001 against all simpler models). However, unlike for *Slwus*$^{CR\text{-}lc}$ where the allele-specific effects varied substantially between phenotypically similar genetic backgrounds, the additive model could be rejected in favor of both the constant and proportional epistasis models (likelihood ratio test, p<.0001 for both models), and examination of the estimated epistatic effects between all single and double mutant pairs (table S2) suggested that the *Slcle9* effect varied in a threshold-like manner as a function of *Slclv3*^{Pro} allelic strength. In particular, while *Slcle9* had only a minimal effect on locule in the weaker *Slclv3*^{Pro} backgrounds (which express *SlCLV3* at near wild-type levels, fig. S3), a larger effect emerged in the stronger, higher locule backgrounds where *SlCLV3* is expressed at a substantially lower level (fig. S3), including *Slclv3*^{fas} and the near null mutant *Slclv3*^{28} (Fig. 2B). Based on these observations, we fit an additional model where the *Slcle9* effect increases as a sigmoid function of the strength of the *Slclv3*^{Pro} background (Fig. 2C). Though the idiosyncratic epistasis model still provided a better fit to the data (likelihood ratio test, p<.0001), the sigmoid model provided a better fit than either the constant or proportional epistasis models (likelihood ratio test, p<.0001 against both simpler models). Moreover, if we consider the epistatic variance in log locule number as the fraction of the variance that is accounted for by the idiosyncratic epistasis model but not accounted by the additive model, we find that the sigmoid model captures the vast majority of this variance (90.0%, table S2). We thus conclude that while there is a statistically significant idiosyncratic component

to the *Slcle9* effect, the overall pattern is a dose-dependent saturating relationship, where the effect of *Slcle9* is negligible until a critical *Slclv3*^{Pro} allelic strength (critical degree of *SlCLV3* disruption) is reached. Above this threshold, the effect of *Slcle9* increases and eventually reaches an approximately constant level of enhancement in stronger *Slclv3*^{Pro} backgrounds.

Higher-order mutant combinations reveal additional idiosyncrasy

While our findings show that the effects of *Slcle9* null mutants have a sigmoid epistasis relationship across the *Slclv3*^{Pro} allelic series, modern genotypes typically also carry *Slwus*^{lc} (*31*). To evaluate whether this pattern is maintained in the presence of *Slwus*$^{CR\text{-}lc}$, we constructed and phenotyped a combinatorially complete set of triple mutants using a subset of five mutant *Slclv3*^{Pro} alleles with a wide range of allelic strengths (Fig. 3A, $6 \times 2 \times 2 = 24$ total genotypes). Surprisingly, we found new and unpredicted epistatic interactions in these higher-order mutants that were not present in the double mutants. Though the effect of *Slcle9* on locule number is negligible in wild-type, *Slwus*$^{CR\text{-}lc}$, and weak *Slclv3*^{Pro} mutant backgrounds, locule number was enhanced by *Slcle9* in all triple mutants, including with the weak *Slclv3*$^{Pro\text{-}2}$ allele (Fig. 3A and fig. S2C), and the *Slcle9* effect broadly increased and approached saturation at approximately the level predicted by the sigmoid model (Fig. 3B). Although our previous analyses showed that *Slwus*$^{CR\text{-}lc}$ had a strong positive and negative idiosyncratic influence on the effects of *Slclv3*^{fas} and *Slclv3*$^{Pro\text{-}22}$, respectively (Fig. 1E), we did not observe strong idiosyncratic epistasis with *Slcle9* and these alleles, even though *Slwus*$^{CR\text{-}lc}$ was present in the backgrounds of the triple mutants (Fig. 3 and table S2). In contrast, we observed a striking reversal of the *Slcle9* effect on *Slclv3*$^{Pro\text{-}11}$ in the presence of *Slwus*$^{CR\text{-}lc}$, where locule number is actually decreased, instead of increased, by the *Slcle9* mutation (Fig. 3B). Consistent with this new idiosyncratic effect, the constant and proportional epistasis models were rejected in favor of the idiosyncratic epistasis model (likelihood ratio test, $p<.0001$ against both simpler models). Taken together, these findings demonstrate that the predictability of epistatic effects and phenotypic outcomes in two-way interactions can be altered in higher-order allelic combinations.

Discussion

Cryptic mutations, which have subtle or no effect on phenotype (*37*), are pervasive in genomes, and despite little knowledge about the underlying genes, alleles, and mechanisms, these cryptic background mutations are widely recognized as critical factors that shape the evolutionary trajectories of traits under both natural and artificial selection (*2*, *38–40*). Our observations expose the dynamic role played by epistasis among the natural and cryptic alleles of these genes during tomato domestication. The natural hypomorphic *SlCLE9* allele pre-existed as a cryptic variant in the genome of the wild progenitor of tomato (*27*, *29*), and was followed by *Slwus*^{lc}, whose subtle influence on locule number likely also persisted cryptically (*31*). Consequently, the later emergence of *Slclv3*^{fas} would have immediately triggered a positive idiosyncratic epistatic interaction with *Slwus*^{lc} wherein these new *Slclv3*^{fas} mutants displayed a marked increase in locule number that they would not have shown in the absence of these preceding mutations. Thus, the fortuitous *SLCLV3* cis-regulatory allele responsible for the initial and most consequential step in enhancing fruit size by increasing locule number during domestication appears to have had its quantitative effect due to a combination of an unpredictable idiosyncratic interaction with the cryptic gain-of-function *Slwus*^{lc} allele as well as alleviation of dose-dependent suppression by the cryptic hypomorphic *SlCLE9*.

The idiosyncratic epistatic effects that we observe here are presumably driven by allele-specific differences in the composition and location of regulatory elements within the *SlCLV3*

promoter. However, identifying the causative regulatory elements is difficult both because each mutant allele typically disrupts dozens of transcription factor binding sites (*28*), and because the regulatory architecture of meristem development remains incompletely understood (*24*). In light of the remarkable complexity of epistatic interactions arising from a limited number of background mutations and a one-dimensional array of allelic strength, our findings hold ramifications for other organisms and phenotypes, in both natural genetic contexts and genetic engineering. Gene regulatory networks are the foundation of biological systems (*41*, *42*), and these networks depend on intricate signaling and feedback mechanisms, encompassing both positive and negative regulation, between genes and their protein products, often involving paralogs engaged in asymmetrical redundancy relationships (*3*, *30*, *43*). Notably, the redundancy relationship between *SlCLV3* and *SlCLE9* is based on a widespread transcriptional compensation mechanism (*27*, *29*, *43*, *44*), suggesting that similar saturating dose-dependent epistatic interactions are likely to be ubiquitous. However, varying allelic states of redundant paralogs could affect the form of dose-dependent relationships. For example, *SlCLE9* orthologues differ across Solanaceae crops, from the more potent partner of the *SlCLV3* orthologue in groundcherry to the complete loss of this gene in eggplant (*29*). These varying allelic states are important to consider when designing editing strategies to increase locule number. Likewise, how epistasis is transformed across an allelic series could also be influenced by environmental conditions. We found that the phenotypic effects of both coding and regulatory *SlCLV3* mutations are typically not affected substantially by the environment (*28*), and although the patterns of epistasis observed in our study might have some dependence on environment, the genotype-specific locule number distributions remained remarkably consistent across different field seasons and locations (fig. S2). Importantly, employing similar methods to those used here provides a path to determine the form of these interactions for other organisms, traits and environments, which would facilitate the fine-tuning of phenotypes in a controlled and quantitative manner.

It is important to acknowledge, however, that the predictability of outcomes when engineering novel alleles and allelic combinations may be influenced by idiosyncratic interactions with other background mutations (*2*, *45*, *46*). Indeed, our observation of a new idiosyncratic effect in the $Slclv3^{Pro}$ $Slwus^{lc}$ *Slcle9* triple mutants, which was not present in the $Slclv3^{Pro}$ $Slwus^{lc}$ double mutants, underscores how predictability of effects from engineered alleles may decay in increasingly divergent genetic backgrounds. A related issue is that natural alleles responsible for phenotypic differences between genotypes and species, which are being increasingly revealed through pan-genomics (*32*, *33*, *47*, *48*), may be enriched for idiosyncratic effects due to the action of natural or artificial selection (*49*, *50*), as seen with $Slclv3^{fas}$ and $Slwus^{lc}$. More broadly, the expected degree of variability in epistatic interactions displayed by different alleles at the same locus, how these epistatic interactions are transformed as a function of allelic strength, and whether these patterns differ between natural versus artificial alleles and regulatory versus coding sequences remain as open questions. While we have shown that our $Slclv3^{Pro}$ allelic series interacts differently with $Slwus^{lc}$ (idiosyncratically) versus *Slcle9* (a systematic, dose-dependent response), it will be informative to investigate whether other allelic series will exhibit consistent or distinct patterns of epistatic interaction when the same allelic series is paired with different epistatic partners. Systematic mapping of predictable epistatic interactions, while either minimizing or perhaps leveraging potential idiosyncratic effects, represents a key challenge in current and future endeavors to modify, correct, and optimize traits in agriculture and human health.

References and Notes

1. T. F. C. Mackay, Epistasis and quantitative traits: using model organisms to study gene–gene interactions. *Nat Rev Genet 2013 151*. **15**, 22–33 (2013).
2. T. B. Sackton, D. L. Hartl, Genotypic Context and Epistasis in Individuals and Populations. *Cell*. **166**, 279–287 (2016).
3. B. Lehner, Molecular mechanisms of epistasis within and between genes. *Trends Genet*. **27**, 323–331 (2011).
4. R. F. Campbell, P. T. McGrath, A. B. Paaby, Analysis of Epistasis in Natural Traits Using Model Organisms. *Trends Genet*. **34**, 883–898 (2018).
5. A. N. Nguyen Ba, K. R. Lawrence, A. Rego-Costa, S. Gopalakrishnan, D. Temko, F. Michor, M. M. Desai, Barcoded Bulk QTL mapping reveals highly polygenic and epistatic architecture of complex traits in yeast. *Elife*. **11** (2022).
6. N. Bosch-Guiteras, J. van Leeuwen, Exploring conditional gene essentiality through systems genetics approaches in yeast. *Curr Opin Genet Dev*. **76**, 101963 (2022).
7. M. Costanzo, B. VanderSluis, E. N. Koch, A. Baryshnikova, C. Pons, G. Tan, W. Wang, M. Usaj, J. Hanchard, S. D. Lee, V. Pelechano, E. B. Styles, M. Billmann, J. Van Leeuwen, N. Van Dyk, Z. Y. Lin, E. Kuzmin, J. Nelson, J. S. Piotrowski, T. Srikumar, S. Bahr, Y. Chen, R. Deshpande, C. F. Kurat, S. C. Li, Z. Li, M. M. Usaj, H. Okada, N. Pascoe, B. J. S. Luis, S. Sharifpoor, E. Shuteriqi, S. W. Simpkins, J. Snider, H. G. Suresh, Y. Tan, H. Zhu, N. Malod-Dognin, V. Janjic, N. Przulj, O. G. Troyanskaya, I. Stagljar, T. Xia, Y. Ohya, A. C. Gingras, B. Raught, M. Boutros, L. M. Steinmetz, C. L. Moore, A. P. Rosebrock, A. A. Caudy, C. L. Myers, B. Andrews, C. Boone, A global genetic interaction network maps a wiring diagram of cellular function. *Science*. **353** (2016)
8. M. S. Johnson, M. M. Desai, Mutational robustness changes during long-term adaptation in laboratory budding yeast populations. *Elife*. **11** (2022).
9. E. Caudal, A. Friedrich, A. Jallet, M. Garin, J. Hou, J. Schacherer, Loss-of-function mutation survey revealed that genes with background-dependent fitness are rare and functionally related in yeast. *Proc Natl Acad Sci U S A*. **119**, e2204206119 (2022).
10. R. M. L. Ang, S.-A. A. Chen, A. F. Kern, Y. Xie, H. B. Fraser, Widespread epistasis among beneficial genetic variants revealed by high-throughput genome editing. *Cell Genomics*. **3**, 100260 (2023).
11. T. M. Norman, M. A. Horlbeck, J. M. Replogle, A. Y. Ge, A. Xu, M. Jost, L. A. Gilbert, J. S. Weissman, Exploring genetic interaction manifolds constructed from rich single-cell phenotypes. *Science*. **365**, 786–793 (2019).
12. M. A. Horlbeck, A. Xu, M. Wang, N. K. Bennett, C. Y. Park, D. Bogdanoff, B. Adamson, E. D. Chow, M. Kampmann, T. R. Peterson, K. Nakamura, M. A. Fischbach, J. S. Weissman, L. A. Gilbert, Mapping the Genetic Landscape of Human Cells. *Cell*. **174**, 953-967.e22 (2018).
13. J. Shi, E. Wang, J. P. Milazzo, Z. Wang, J. B. Kinney, C. R. Vakoc, Discovery of cancer drug targets by CRISPR-Cas9 screening of protein domains. *Nat Biotechnol*. **33**, 661–667 (2015).
14. H. J. Liu, L. Jian, J. Xu, Q. Zhang, M. Zhang, M. Jin, Y. Peng, J. Yan, B. Han, J. Liu, F. Gao, X. Liu, L. Huang, W. Wei, Y. Ding, X. Yang, Z. Li, M. Zhang, J. Sun, M. Bai, W. Song, H. Chen, X. Sun, W. Li, Y. Lu, Y. Liu, J. Zhao, Y. Qian, D. Jackson, A. R. Fernie, J. Yan, High-Throughput CRISPR/Cas9 Mutagenesis Streamlines Trait Gene Identification in Maize. *Plant Cell*. **32**, 1397–1413 (2020).
15. Y. Hu, P. Patra, O. Pisanty, A. Shafir, Z. M. Belew, J. Binenbaum, S. Ben Yaakov, B. Shi,

L. Charrier, G. Hyams, Y. Zhang, M. Trabulsky, O. Caldararu, D. Weiss, C. Crocoll, A. Avni, T. Vernoux, M. Geisler, H. H. Nour-Eldin, I. Mayrose, E. Shani, Multi-Knock—a multi-targeted genome-scale CRISPR toolbox to overcome functional redundancy in plants. *Nat Plants 2023 94*. **9**, 572–587 (2023).

16. P. J. Wittkopp, G. Kalay, Cis -regulatory elements: molecular mechanisms and evolutionary processes underlying divergence. *Nat Rev Genet*. **13**, 59–69 (2012).
17. A. P. Marand, A. L. Eveland, K. Kaufmann, N. M. Springer, cis-Regulatory Elements in Plant Development, Adaptation, and Evolution. *https://doi.org/10.1146/annurev-arplant-070122-030236*. **74** (2023), doi:10.1146/ANNUREV-ARPLANT-070122-030236.
18. H. K. Long, S. L. Prescott, J. Wysocka, Ever-Changing Landscapes: Transcriptional Enhancers in Development and Evolution. *Cell*. **167**, 1170–1187 (2016).
19. F. W. Albert, L. Kruglyak, The role of regulatory variation in complex traits and disease. *Nat Rev Genet 2015 164*. **16**, 197–212 (2015).
20. W. Schwarzer, F. Spitz, The architecture of gene expression: integrating dispersed cis-regulatory modules into coherent regulatory domains. *Curr Opin Genet Dev*. **27**, 74–82 (2014).
21. S. Kim, J. Wysocka, Deciphering the multi-scale, quantitative cis-regulatory code. *Mol Cell*. **83**, 373–392 (2023).
22. T. Fuqua, J. Jordan, M. E. van Breugel, A. Halavatyi, C. Tischer, P. Polidoro, N. Abe, A. Tsai, R. S. Mann, D. L. Stern, J. Crocker, Dense and pleiotropic regulatory information in a developmental enhancer. *Nature*. **587**, 235–239 (2020).
23. J. H. Massey, J. Li, D. L. Stern, P. J. Wittkopp, Distinct genetic architectures underlie divergent thorax, leg, and wing pigmentation between Drosophila elegans and D. gunungcola. *Hered 2021 1275*. **127**, 467–474 (2021).
24. M. Kitagawa, D. Jackson, Control of Meristem Size. *https://doi.org/10.1146/annurev-arplant-042817-040549*. **70**, 269–291 (2019).
25. H. Schoof, M. Lenhard, A. Haecker, K. F. X. Mayer, G. Jürgens, T. Laux, The Stem Cell Population of Arabidopsis Shoot Meristems Is Maintained by a Regulatory Loop between the CLAVATA and WUSCHEL Genes. *Cell*. **100**, 635–644 (2000).
26. D. Rodríguez-Leal, Z. H. Lemmon, J. Man, M. E. Bartlett, Z. B. Lippman, Engineering Quantitative Trait Variation for Crop Improvement by Genome Editing. *Cell*. **171**, 470-480.e8 (2017).
27. D. Rodriguez-Leal, C. Xu, C.-T. Kwon, C. Soyars, E. Demesa-Arevalo, J. Man, L. Liu, Z. H. Lemmon, D. S. Jones, J. Van Eck, D. P. Jackson, M. E. Bartlett, Z. L. Nimchuk, Z. B. Lippman, Evolution of buffering in a genetic circuit controlling plant stem cell proliferation. *Nat Genet*, 1 (2019).
28. X. Wang, L. Aguirre, D. Rodríguez-Leal, A. Hendelman, M. Benoit, Z. B. Lippman, Dissecting cis-regulatory control of quantitative trait variation in a plant stem cell circuit. *Nat Plants*. **7**, 419–427 (2021).
29. C.-T. Kwon, L. Tang, X. Wang, I. Gentile, A. Hendelman, G. Robitaille, J. Van Eck, C. Xu, Z. B. Lippman, Dynamic evolution of small signalling peptide compensation in plant stem cell control. *Nat Plants 2022 84*. **8**, 346–355 (2022).
30. G. C. Briggs, K. S. Osmont, C. Shindo, R. Sibout, C. S. Hardtke, Unequal genetic redundancies in Arabidopsis – a neglected phenomenon? *Trends Plant Sci*. **11**, 492–498 (2006).
31. L. Pereira, L. Zhang, M. Sapkota, A. Ramos, H. Razifard, A. L. Caicedo, E. van der Knaap, Unraveling the genetics of tomato fruit weight during crop domestication and diversification. *Theor Appl Genet*. **134**, 3363–3378 (2021).

32. M. Alonge, X. Wang, M. Benoit, S. Soyk, L. Pereira, L. Zhang, H. Suresh, S. Ramakrishnan, F. Maumus, D. Ciren, Y. Levy, T. H. Harel, G. Shalev-Schlosser, Z. Amsellem, H. Razifard, A. L. Caicedo, D. M. Tieman, H. Klee, M. Kirsche, S. Aganezov, T. R. Ranallo-Benavidez, Z. H. Lemmon, J. Kim, G. Robitaille, M. Kramer, S. Goodwin, W. R. McCombie, S. Hutton, J. Van Eck, J. Gillis, Y. Eshed, F. J. Sedlazeck, E. van der Knaap, M. C. Schatz, Z. B. Lippman, Major Impacts of Widespread Structural Variation on Gene Expression and Crop Improvement in Tomato. *Cell*. **182**, 145-161.e23 (2020).
33. Y. Zhou, Z. Zhang, Z. Bao, H. Li, Y. Lyu, Y. Zan, Y. Wu, L. Cheng, Y. Fang, K. Wu, J. Zhang, H. Lyu, T. Lin, Q. Gao, S. Saha, L. Mueller, Z. Fei, T. Städler, S. Xu, Z. Zhang, D. Speed, S. Huang, Graph pangenome captures missing heritability and empowers tomato breeding. *Nat 2022 6067914*. **606**, 527–534 (2022).
34. T. F. Hansen, G. P. Wagner, Modeling Genetic Architecture: A Multilinear Theory of Gene Interaction. *Theor Popul Biol*. **59**, 61–86 (2001).
35. C. W. Bakerlee, A. N. Nguyen Ba, Y. Shulgina, J. I. Rojas Echenique, M. M. Desai, Idiosyncratic epistasis leads to global fitness–correlated trends. *Science*. **376**, 630–635 (2022).
36. D. M. Lyons, Z. Zou, H. Xu, J. Zhang, Idiosyncratic epistasis creates universals in mutational effects and evolutionary trajectories. *Nat Ecol Evol*. **4**, 1685–1693 (2020).
37. A. B. Paaby, M. V. Rockman, Cryptic genetic variation: evolution's hidden substrate. *Nat Rev Genet 2014 154*. **15**, 247–258 (2014).
38. K. Mcguigan, N. Nishimura, M. Currey, D. Hurwit, W. A. Cresko, Cryptic genetic variation and body size evolution in threespine stickleback. *Evolution (N Y)*. **65**, 1203–1211 (2011).
39. J. Hou, J. van Leeuwen, B. J. Andrews, C. Boone, Genetic Network Complexity Shapes Background-Dependent Phenotypic Expression. *Trends Genet*. **34**, 578 (2018).
40. N. Lauter, J. Doebley, Genetic variation for phenotypically invariant traits detected in teosinte: implications for the evolution of novel forms. *Genetics*. **160**, 333 (2002).
41. M. Fagny, F. Austerlitz, Polygenic Adaptation: Integrating Population Genetics and Gene Regulatory Networks. *Trends Genet*. **37**, 631–638 (2021).
42. M. Costanzo, E. Kuzmin, J. van Leeuwen, B. Mair, J. Moffat, C. Boone, B. Andrews, Global Genetic Networks and the Genotype-to-Phenotype Relationship. *Cell*. **177**, 85–100 (2019).
43. R. Kafri, M. Springer, Y. Pilpel, Genetic Redundancy: New Tricks for Old Genes. *Cell*. **136**, 389–392 (2009).
44. G. Diss, D. Ascencio, A. Deluna, C. R. Landry, Molecular mechanisms of paralogous compensation and the robustness of cellular networks. *J Exp Zool Part B Mol Dev Evol*. **322**, 488–499 (2014).
45. F. J. Yuste-Lisbona, A. Fernández-Lozano, B. Pineda, S. Bretones, A. Ortíz-Atienza, B. García-Sogo, N. A. Müller, T. Angosto, J. Capel, V. Moreno, J. M. Jiménez-Gómez, R. Lozano, ENO regulates tomato fruit size through the floral meristem development network. *Proc Natl Acad Sci*. **117**, 8187–8195 (2021).
46. X. Song, X. Meng, H. Guo, Q. Cheng, Y. Jing, M. Chen, G. Liu, B. Wang, Y. Wang, J. Li, H. Yu, Targeting a gene regulatory element enhances rice grain yield by decoupling panicle number and size. *Nat Biotechnol 2022*, 1–9 (2022).
47. P. E. Bayer, A. A. Golicz, A. Scheben, J. Batley, D. Edwards, Plant pan-genomes are the new reference. *Nat Plants 2020 68*. **6**, 914–920 (2020).
48. R. M. Sherman, S. L. Salzberg, Pan-genomics in the human genome era. *Nat Rev Genet 2020 214*. **21**, 243–254 (2020).

49. J. A. Draghi, J. B. Plotkin, Selection biases the prevalence and type of epistasis along adaptive trajectories. *Evolution (N Y)*. **67**, 3120–3131 (2013).
50. J. Doebley, A. Stec, C. Gustus, teosinte branched1 and the origin of maize: evidence for epistasis and the evolution of dominance. *Genetics*. **141**, 333–346 (1995).
51. L. Aguirre, A. Hendelman, S. F. Hutton, D. M. McCandlish, Z. B. Lippman, Data for: Idiosyncratic and dose-dependent epistasis drives variation in tomato fruit size, *Zenodo* (2023); https://doi.org/10.5281/zenodo.8267283.
52. S. J. Park, K. Jiang, M. C. Schatz, Z. B. Lippman, Rate of meristem maturation determines inflorescence architecture in tomato. *Proc Natl Acad Sci U S A*. **109**, 639–644 (2012).

Acknowledgments: We thank members of the Lippman laboratory for comments and discussions and assisting with phenotyping. We thank M. Bartlett and Y. Eshed for helpful discussions. We thank B. Semen, and G. Robitaille from the Lippman lab for technical support. We thank T. Mulligan, K. Schlecht, A. Krainer, S. Qiao, and B. Fitzgerald for assistance with plant care.

Funding:

National Science Foundation Graduate Research Fellowship grant 1938105 (LA)

William Randolph Hearst Foundation Scholarship (LA)

National Institutes of Health grant R35GM133613 (DMM)

Alfred P. Sloan Research Fellowship (DMM)

National Science Foundation Plant Genome Research Program grant IOS-2129189 (ZBL)

The Howard Hughes Medical Institute (ZBL)

Author contributions:

Conceptualization: DMM, ZBL

Methodology: LA, SFH, DMM, ZBL

Investigation: LA, SFH, AH, DMM, ZBL

Visualization: LA, AH, DMM, ZBL

Funding acquisition: LA, DMM, ZBL

Supervision: ZBL

Writing – original draft: LA, AH, DMM, ZBL

Writing – review & editing: LA, AH, DMM, ZBL

Competing interests: Authors declare that they have no competing interests.

Data and materials availability: Source code for statistical analysis of epistasis models can be found on Zenodo (51). All data are available in the main text or the supplementary materials.

Supplementary Materials

Materials and Methods

Figs. S1 to S3

Tables S1 to S4

Reference 52

Fig. 1. A promoter allelic series of the fruit size gene *SlCLV3* reveals idiosyncratic epistasis. (**A**) The *SlWUS-SlCLV3* circuit and the paralog *SlCLE9* control locule number. Fruits of wild type (WT, left) and *Slclv3*^{fas} *Slwus*^{lc} double mutants (right). Dashed lines and numbers indicate locules. (**B**) Experimental design. (**C**) Heatmap of *SlCLV3* promoter region encompassing 11 *Slclv3* promoter (*Slclv3*^{Pro}) alleles. Purple intensity in 20 bp windows indicates ratios of sequence change relative to WT (cyan). Red: inversion. Stacked bar charts are percentage of fruits having each locule number range. White/Gray boxes indicate WT and mutant genotype for each gene, respectively. Replicated plants/fruits (N/*n*). (**D**) Epistasis models between *Slwus*$^{CR\text{-}lc}$ and the *Slclv3*^{Pro} alleles, depicted by plotting percent change of double mutants against mean log locule numbers of *Slclv3*^{Pro} mutants. Combined effect of *Slwus*^{lc} and *Slclv3*^{fas} is indicated. (**E**) *Slwus*$^{CR\text{-}lc}$ effect on mean log locule number (*Slwus*$^{CR\text{-}lc}$ *Slclv3*^{Pro} genotypes compared to *SlWUS*^{LC} *Slclv3*^{Pro} genotypes), plotted against mean log locule number of the corresponding *SlWUS*^{LC} *Slclv3*^{Pro} genetic background (error bars indicate ±1 standard error). Data are from two replicated trials, except for *Slclv3*$^{Pro\text{-}28}$ (see also fig. S2A, and tables S2 and S3). Red arrows show strongest idiosyncratic effects, including positive synergism between *Slclv3*^{fas} and *Slwus*^{lc}.

Fig. 2. The compensating paralog *SlCLE9* interacts with *SlCLV3* in a sigmoidal dose-dependent epistasis relationship. (**A**) Stacked bar charts show percentage of total fruits for each locule number range of *Slclv3*^{Pro} single and *Slclv3*^{Pro} *Slcle9* double mutant alleles. White/Gray boxes indicate WT and mutant genotype for each gene, respectively. Number of replicated plants/number fruits (N/*n*). (**B**) Representative fruit images and locule number quantification (mean ±1 standard deviation) showing the effect of *Slcle9* on locule number in WT and the *Slclv3*^{Pro} mutants. Scale bars: 1 cm. (**C**) *Slcle9* effect on mean log locule number (*Slcle9* *Slclv3*^{Pro} double mutants as compared to *SlCLE9* *Slclv3*^{Pro} single mutants), plotted against the mean log locule number of the corresponding *SlCLE9* *Slclv3*^{Pro} genetic background (error bars indicate ±1 standard error). Black line indicates the maximum likelihood fit for the sigmoid model. Data are from three replicate trials (see also fig. S2B and tables S2 and S3).

Fig. 3. Loss of *SlCLE9* imposes new and unpredicted idiosyncratic effects on *Slclv3*^{Pro} *Slwus*$^{CR\text{-}lc}$ backgrounds. (**A**) Stacked bar charts show percentage of total fruits for each locule number range of WT and all indicated single, double, and triple mutant genotypes. White/Gray boxes indicate WT and mutant genotype for each gene, respectively. Number of replicated plants/fruits (N/*n*). (**B**) *Slcle9* effect on the log mean locule number (*Slcle9* *Slwus*$^{CR\text{-}lc}$ *Slclv3*^{Pro} triple mutants as compared to the *SlCLE9* *Slwus*$^{CR\text{-}lc}$ *Slclv3*^{Pro} double mutants) in the indicated *SlCLE9* *Slwus*$^{CR\text{-}lc}$ *Slclv3*^{Pro} double mutant background (error bars indicate ±1 standard error). Notice the strong negative idiosyncratic epistasis in the *Slclv3*$^{Pro\text{-}11}$ *Slwus*$^{CR\text{-}lc}$ background. Black line indicates no effect and the red dashed line indicates the saturated effect of *Slcle9* on *Slclv3*^{Pro} based on our previously fit sigmoid model (see also Fig. 2C, fig. S2C and tables S2 and S3).

Figure 1

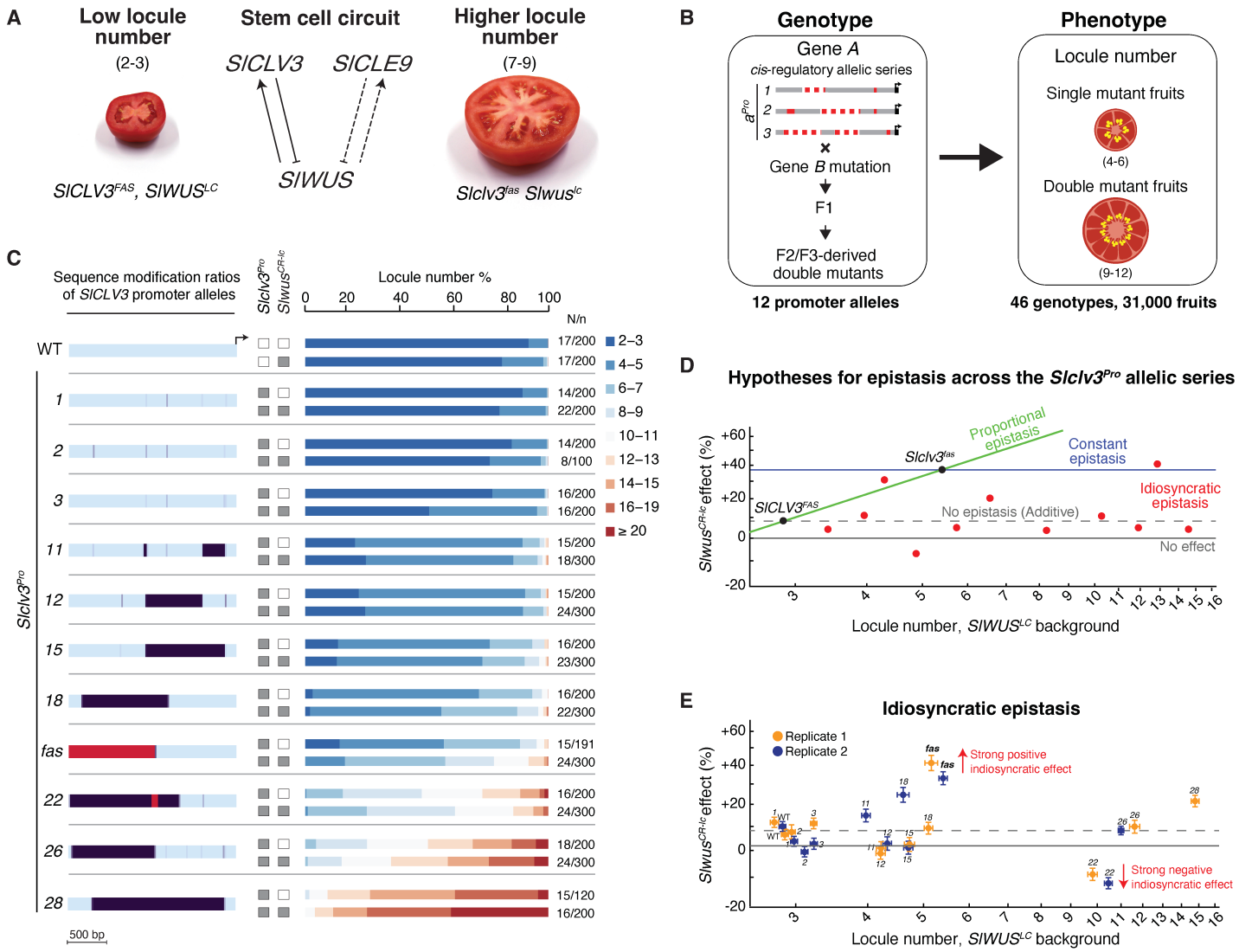
A
Low locule number
(2-3)
SlCLV3FAS, SlWUSLC
Stem cell circuit
SlCLV3
SlCLE9
SlWUS
Higher locule number
(7-9)
Slclv3fas Slwuslc
B
Genotype
Gene A
cis-regulatory allelic series
aPro
1
2
3
Gene B mutation
F1
F2/F3-derived double mutants
12 promoter alleles
Phenotype
Locule number
Single mutant fruits
(4-6)
Double mutant fruits
(9-12)
46 genotypes, 31,000 fruits
C
Sequence modification ratios of SlCLV3 promoter alleles
Slclv3Pro
SlwusCR-lc
Locule number %
0 20 40 60 80 100
N/n
WT
1
2
3
11
12
15
18
fas
22
26
28
17/200
17/200
14/200
22/200
14/200
8/100
16/200
16/200
15/200
18/300
15/200
24/300
16/200
23/300
16/200
22/300
15/191
24/300
16/200
24/300
18/200
24/300
15/120
16/200
2–3
4–5
6–7
8–9
10–11
12–13
14–15
16–19
≥ 20
500 bp
D
Hypotheses for epistasis across the Slclv3Pro allelic series
SlwusCR-lc effect (%)
+60
+40
+20
0
-20
Proportional epistasis
Constant epistasis
Idiosyncratic epistasis
No epistasis (Additive)
No effect
Slclv3fas
SlCLV3FAS
3 4 5 6 7 8 9 10 11 12 13 14 15 16
Locule number, SlWUSLC background
E
Idiosyncratic epistasis
Replicate 1
Replicate 2
Strong positive indiosyncratic effect
Strong negative indiosyncratic effect
SlwusCR-lc effect (%)
+60
+40
+20
0
-20
3 4 5 6 7 8 9 10 11 12 13 14 15 16
Locule number, SlWUSLC background

Figure 2

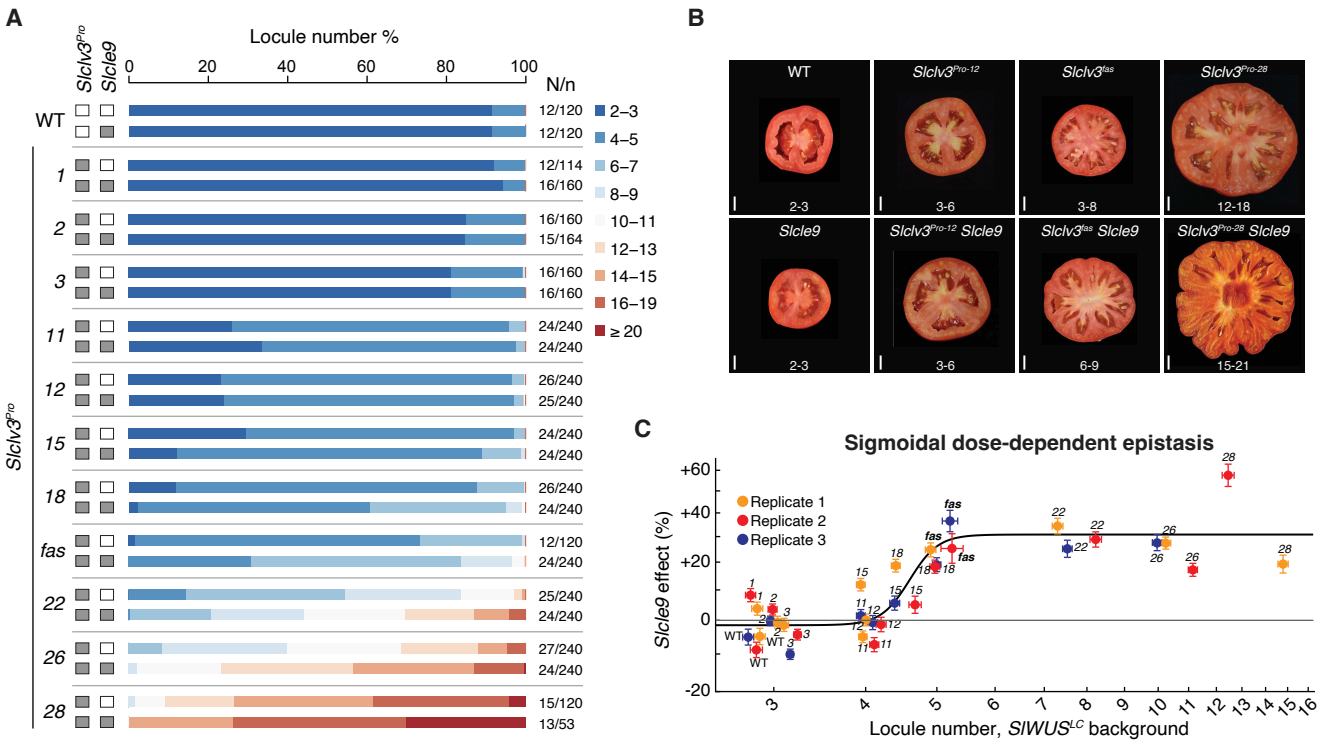
A
Locule number %
0
20
40
60
80
100
N/n
SlclvPro
Slcle9
WT
1
2
3
11
12
15
18
fas
22
26
28
12/120
12/120
12/114
16/160
16/160
15/164
16/160
16/160
24/240
24/240
26/240
25/240
24/240
24/240
26/240
24/240
12/120
24/240
25/240
24/240
27/240
24/240
15/120
13/53
2–3
4–5
6–7
8–9
10–11
12–13
14–15
16–19
≥ 20
B
WT
SlclvPro-12
Slclvfas
SlclvPro-28
Slcle9
SlclvPro-12 Slcle9
Slclvfas Slcle9
SlclvPro-28 Slcle9
2-3
3-6
3-8
12-18
2-3
3-6
6-9
15-21
C
Sigmoidal dose-dependent epistasis
Replicate 1
Replicate 2
Replicate 3
Slcle9 effect (%)
+60
+40
+20
0
-20
Locule number, SlWUSLC background

Figure 3

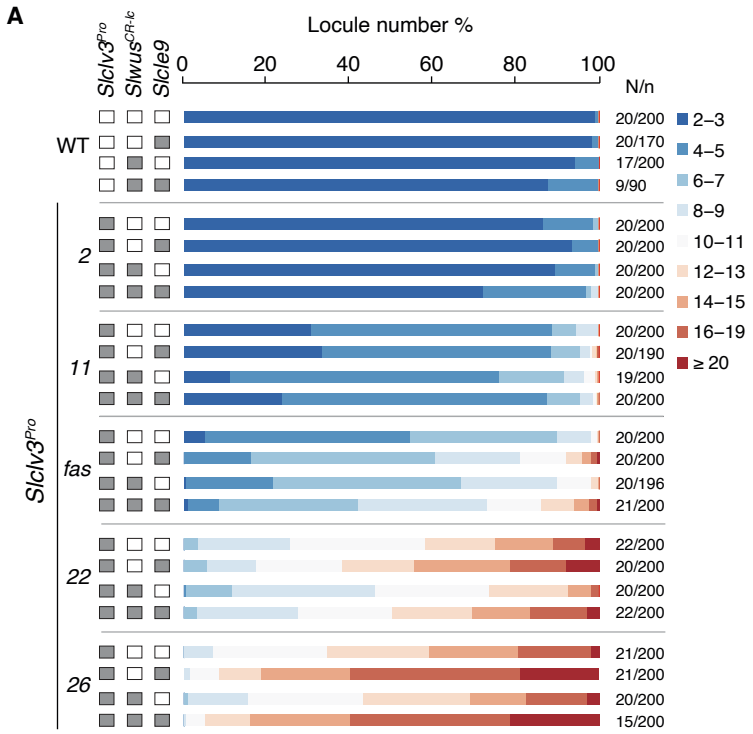
A
Locule number %
0
20
40
60
80
100
N/n
SlclV3Pro
SlwusCR-lc
Slcle9
WT
2
11
fas
22
26
20/200
20/170
17/200
9/90
20/200
20/200
20/200
20/200
20/200
20/190
19/200
20/200
20/200
20/200
20/196
21/200
22/200
20/200
20/200
22/200
21/200
21/200
20/200
15/200
2–3
4–5
6–7
8–9
10–11
12–13
14–15
16–19
≥ 20

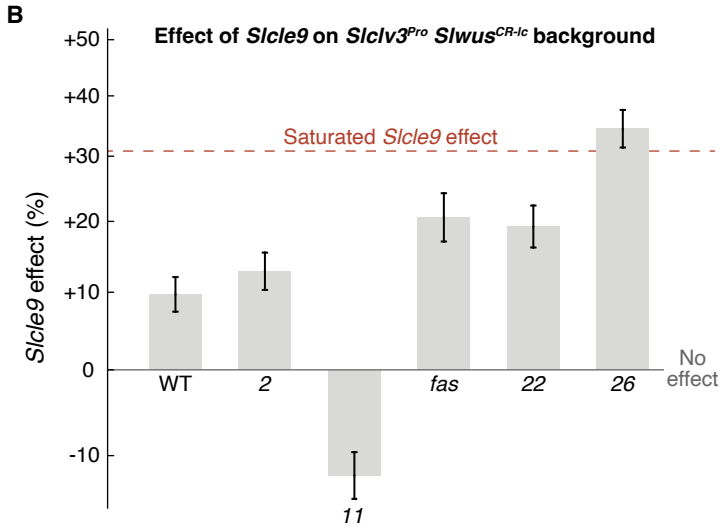
B
Effect of Slcle9 on SlclV3Pro SlwusCR-lc background
Slcle9 effect (%)
+50
+40
+30
+20
+10
0
-10
Saturated Slcle9 effect
No effect
WT
2
11
fas
22
26

Science
AAAS

Supplementary Materials for

Idiosyncratic and dose-dependent epistasis drives variation in tomato fruit size

Lyndsey Aguirre[1], Anat Hendelman[2], Samuel F. Hutton[3], David M. McCandlish[2*], Zachary B. Lippman[1,2,4*]

Corresponding authors: mccandlish@cshl.edu, lippman@cshl.edu

The PDF file includes:

Materials and Methods
Figs. S1 to S3
Tables S1 to S4
References 52

Materials and Methods

Plant material and genotyping

Seeds of wild type (*Solanum lycopersicum* cultivar M82, LA3475), *Slwus*$^{CR\text{-}lc}$ (*Solyc02g083950*), *Slcle9* (*Solyc06g074060*), and *Slclv3*, *Slclv3*^{Pro} including *Slclv3*^{fas} (*Solyc11g071380*) alleles in the M82 background were from our own stocks. *Slwus*$^{CR\text{-}lc}$, *Slclv3*, *Slclv3*^{Pro}, *Slclv3*^{fas}, and *Slcle9* mutant alleles were described before (*26-28*).

All *Slclv3*^{Pro} alleles were generated by our CRISPR-Cas9 mutagenesis drive system (26), Briefly, Cas9 positive F1 *Slclv3*^{Pro} plants were grown in the field at Uplands Farm of Cold Spring Harbor Laboratory, New York. F2 progeny plants were genotyped for both *Cas9* and the *SlCLV3* targeted-promoter region to identify non-transgenic, biallelic, and homozygous plants carrying new alleles (primer sequences for genotyping are listed in table S4). Sequencing of new alleles was performed for at least three cloned individuals per putative allele (StrataClone Blunt PCR Cloning Kit, Agilent). Sequences were assembled using Geneious (v.11.1.5) software. To eliminate potential rare CRISPR-Cas9 off-target mutations and to mitigate effects from potential background mutations, homozygous *Slclv3*^{Pro} alleles were isolated from multiple backcrosses to WT and were verified by PCR to no longer contain the *Cas9* transgene. These homozygous *Slclv3*^{Pro} alleles were then used in crosses to both *Slwus*$^{CR\text{-}lc}$ and *Slcle9,* both of which were also generated in the same near isogenic M82 background. *Slclv3*^{Pro} *Slwus*$^{CR\text{-}lc}$ and *Slclv3*^{Pro} *Slcle9* double homozygous individuals were isolated then in the F2 generation, and in later generations, were used in subsequent comparative quantitative locule phenotyping (Fig. S1) as well as in further crosses to generate *Slclv3*^{Pro} *Slwus*$^{CR\text{-}lc}$ *Slcle9* triple homozygous mutants. Due to the phenotypic severity of the *Slclv3*$^{Pro\text{-}29}$ allele, seed stocks for the S*lclv3*$^{Pro\text{-}29}$ *Slwus*$^{CR\text{-}lc}$ *Slcle9* triple mutant were maintained with segregation of the S*lclv3*$^{Pro\text{-}29\ +/-}$ allele in the background of *Slwus*$^{CR\text{-}lc}$ *Slcle9*, and triple homozygous mutant plants for this allele were isolated genotypically in each generation and were verified phenotypically by the severity of both vegetative and fruit fasciation.

Growth conditions and phenotyping

Seeds were either germinated on moistened filter paper at 28 °C in the dark and later transferred to soil at three days post germination (dpg) or directly sown in soil in 96-cell plastic flats and grown to 4~5-week-old seedlings in the greenhouse. Seedlings were then transplanted to 4L pots in the greenhouse for crossing purposes or directly to the fields at Cold Spring Harbor Laboratory, New York or at The University of Florida Gulf Coast Research and Education Center. The greenhouse condition is long-day (16 h light, 26-28 °C / 8 h dark, 18-20 °C; 40-60% relative humidity) with natural light supplemented with artificial light from high-pressure sodium bulbs (~250 µmol m^{-2} s^{-1}). Plants in the fields were grown under drip irrigation and standard fertilizer regimes, and were used for quantifications of fruit locule number. To quantify fruit locule number, fruits were harvested from multiple inflorescences and dissected horizontally to allow quantification of locule number. For each genotype, locules were counted from ~100-300 fruits from ~15-30 individual plants on average (table S3). For the *Slclv3*$^{Pro\text{-}29}$ *Slcle9* double mutants and the *Slclv3*$^{Pro\text{-}29}$ *Slwus*$^{CR\text{-}lc}$ *Slcle9* triple mutants, fruit set was low due to fertility defects from severe fasciation. Fruit locule counts for these genotypes were either aggregated from all seasons and treated as a single replicate (fig. S2B) or carpel numbers were counted from flowers to supplement for low locule count data (fig. S2C). To quantify ovary carpel number, ovaries from multiple inflorescences were dissected under a conventional stereoscope and carpel number was quantified separately from ~10 plants per genotype. As we previously observed that environmental conditions can have minor effects on epistatic relationship among *Slclv3* promoter mutant alleles (28), to

ensure the robustness of our results to environmental variation, for each of the replicated experiments, the plants were grown in two locations (New York and Florida, representing different soil conditions) and over multiple years and growing seasons. For the *Slclv3*^{Pro} *Slwus*$^{CR\text{-}lc}$ experiments, the locule number phenotyping assays were repeated over two independent field seasons: once at Cold Spring Harbor Laboratory's fields in the summer season (2021) and once at The University of Florida-Gulf Coast Research and Education Center fields in the fall season (2021). Locule number assays for the *Slclv3*^{Pro} *Slcle9* experiments were performed once at Cold Spring Harbor Laboratory's fields in the summer season (2020) and twice at The University of Florida-Gulf Coast Research and Education Center fields in the spring season (2020 and 2021). Locule number assays for the *Slclv3*^{Pro} *Slwus*$^{CR\text{-}lc}$ *Slcle9* experiment were also performed at The University of Florida-Gulf Coast Research and Education Center fields in the spring season (2022).

RNA extraction and Quantitative RT-PCR (qPCR)

For gene expression analysis, seeds were germinated on moistened filter paper on Petri dishes at 28 °C in dark. At three dpg, seedlings at a similar developmental stage were transferred to soil in 96-cell plastic flats and grown in the greenhouse. Shoot apices, at the floral meristem developmental stage (meristem maturation staging determined according to (52)), including the first floral meristem and both vegetative and inflorescence sympodial meristems, were collected under a stereoscope and immediately flash-frozen in liquid nitrogen. Seven to ten apices were combined as one biological replicate, and two or three replicates were collected for each genotype. Total RNA was extracted using TRIzol® Reagent (Invitrogen) and 400 ng of total RNA was used for cDNA synthesis using the SuperScript IV VILO Master Mix (Invitrogen). qPCR was performed with gene-specific primers using the Fast SYBR Green Master Mix (Applied Biosystems) reaction system on the QuantStudio 6 Real-Time system (Applied Biosystems). *SlUbiquitin* (*Solyc01g068045*) gene was used as the internal control (all primers used in this study are listed in table S4).

Modeling of epistasis

Because the effects of mutations on locule number interact approximately multiplicatively and the locule number distribution within each line is approximately log-normally distributed, we analyzed the genetic architecture of locule number by conducting least-squares fits on log locule number. More precisely, for each fruit *i* we modeled locule number *yi* as

$$\log(y_i) = \beta_{wt} + \beta_{lc}x_{i,lc} + \beta_{cle9}x_{i,cle9} + \sum_j \beta_j x_{i,j} + \sum_j e_{lc,j}\, x_{i,lc}x_{i,j} + \sum_j e_{cle9,j}x_{i,cle9}x_{i,j} + \mathrm{e}_{lc,cle9}x_{i,lc}x_{i,cle9} + \sum_j e_{lc,cle9,j}\, x_{i,lc}x_{i,\mathrm{cle9}}x_{i,j} + \epsilon_i$$

where β_{wt} controls the wild type locule number, β_{lc} controls the effect of the *Slwus*$^{CR\text{-}lc}$ allele, β_{cle9} controls the effect of the *Slcle9* allele, β_j controls the effect of the *j*-th mutant *Slclv3*^{Pro} allele, $e_{lc,j}$ controls the pairwise interaction between *Slwus*$^{CR\text{-}lc}$ and the *j*-th mutant *Slclv3*^{Pro} allele, $e_{cle9,j}$ controls the pairwise interaction between *Slcle9* and the *j*-th mutant *Slclv3*^{Pro} allele, $e_{lc,cle9}$ controls the pairwise interaction between *Slwus*$^{CR\text{-}lc}$ and *Slcle9*, and $e_{lc,cle9,j}$ controls the three-way interaction between *Slwus*$^{CR\text{-}lc}$, *Slcle9*, and the *j*-th mutant *Slclv3*^{Pro} allele. In the above, the $x_{i,k}$ are indicator variables that take the value 1 if fruit *i* carries allele *k*, and 0 otherwise, and ϵ_i is normally distributed and independent between fruit, with mean 0 and variance σ^2 (so that the maximum likelihood fit of the above model also yields the least squares solution). For the *Slwus*$^{CR\text{-}lc}$ and

Slcle9 experiments, data was pooled across both of the replicates for *Slwus*$^{CR\text{-}lc}$ and all three replicates for *Slcle9*.

While this general model allows a different pairwise and three-way interaction effect for each *Slclv3*^{Pro} allele, we also considered less complex models by constraining the values of the interaction coefficients. Specifically, the non-epistatic model sets the value of all interaction terms $e_{lc,j}$, $e_{cle9,j}$, $e_{lc,cle9}$, and $e_{lc,\,cle9,\,j}$ to 0; the constant epistasis model sets e.g. all the $e_{lc,\,j}$ to the same value; and the proportional epistasis model sets e.g. $e_{lc,\,j} = m\,\beta_j$, where m is a free parameter, so that the magnitude of the epistatic interaction is proportional to the strength of the genetic background. Noting that the proportional and constant epistasis models are nested within the saturated (idiosyncratic epistasis) model and the non-epistatic model is nested within the proportional and constant epistasis models, we compared these models using likelihood ratio tests. For the analysis of the interaction between *Slcle9* and the *Slclv3*^{Pro} alleles, we also considered a model with a saturating interaction term of the form $e_{cle9,j} = a\frac{1}{1+e^{-m\,\beta_j+b}} + c$, which is nested between the constant epistasis and idiosyncratic epistasis models and can arbitrarily closely approximate the proportional epistasis model. For the triple-mutant data we are specifically interested in the effect of *Slcle9* and the interaction between *Slcle9* and the various *Slclv3*^{Pro} mutants when these mutations occur on a *Slwus*$^{CR\text{-}lc}$ background. For the triple mutants, we thus consider only the genotypes containing *Slwus*$^{CR\text{-}lc}$ and fix all of β_{wt}, β_{lc}, β_{cle9} and the β_j to be zero. Then the triple-mutant idiosyncratic epistasis model contains all the remaining terms as free parameters, the proportional epistasis model fixes $e_{lc,\,cle9,\,j} = m\,e_{lc,\,j}$, the constant epistasis model sets all the $e_{lc,\,cle9,\,j}$ equal to the same value, and the no epistasis model sets all the $e_{lc,\,cle9,\,j}$ equal to zero.

In order to provide an additional metric by which to compare these models, we note that the idiosyncratic epistasis model is a fully saturated model with one parameter per genotype and thus captures all possible forms of epistasis, whereas the no epistasis (additive) model does not contain any epistasis. We can therefore quantify the variance in log locule number due to epistasis as the difference between the mean squared error of the idiosyncratic model and the mean squared error of the additive model. The improvement of the mean squared error of any other model relative to the additive model can then be compared to this total epistatic variance to compute the fraction of epistatic variance captured by that model. These values and other metrics of model performance (AICc, BIC) are included in table S2.

Finally, while our main analysis addresses the pattern of epistasis across the *Slclv3*^{Pro} allelic series as a whole, it also may be of interest to ask whether each *Slclv3*^{Pro} mutation has a detectable pairwise or three-way interaction with *Slwus*$^{CR\text{-}lc}$ or *Slcle9* when considered separately from the other *Slclv3*^{Pro} mutations. To answer this question, for each of the three experiments and for each mutant *Slclv3*^{Pro} allele, we fit an additional series of models that included only that particular mutant *Slclv3*^{Pro} allele (table S2). More precisely, for each experiment we fit a series of models of the form:

$$\log(y_i) = \beta_0 + \beta_{lc}x_{i,lc} + \beta_{cle9}x_{i,cle9} + \beta_j x_{i,j} + e_{lc,j}x_{i,lc}x_{i,j} + e_{cle9,j}x_{i,cle9}x_{i,j} + e_{lc,cle9}x_{i,lc}x_{i,cle9} + e_{lc,cle9,j}x_{i,lc}x_{i,\mathrm{cle9}}x_{i,j} + \epsilon_i$$

where the y_i consist of all the data from that experiment that included no mutant *Slclv3*^{Pro} alleles other than the allele of interest *j*. Here, the $x_{i,k}$ take the value -1 if allele *k* is wildtype in fruit *i* and +1 if it is mutant, and β_0 gives the inferred mean phenotype across the four genotypes involved in

a specific pairwise interaction or the 8 genotypes involved in a specific three-way interaction. The additive effect at each locus was then determined by fitting the model with all of the interaction terms set to zero, and the significance of the additive effect was determined via a likelihood ratio test against the model with the corresponding β_k set to zero. Pairwise interaction coefficients were likewise determined by fitting a model where the three-way interaction coefficient $e_{lc,\,cle9,\,j}$ was set to zero and the statistical significance of each pairwise interaction was determined via a likelihood ratio test against a model fit with the corresponding double mutant interaction term set to zero. For the triple-mutant experiment, the significance of the three-way interaction coefficient was determined by a likelihood ratio test against the model with $e_{lc,\,cle9,\,j}$ set to zero. Note that because in this analysis the main effects β_{lc}, and β_{cle9} are determined separately for each of the *Slclv3*^{Pro} mutant alleles, changes in the mutational effects of *Slwus*$^{CR\text{-}lc}$ and *Slcle9* across the allelic series typically appear both as apparent changes in these main effects across the *Slclv3*^{Pro} mutations as well as more explicitly as changes in the magnitude of the estimated interaction terms.

Supplementary Figure 1

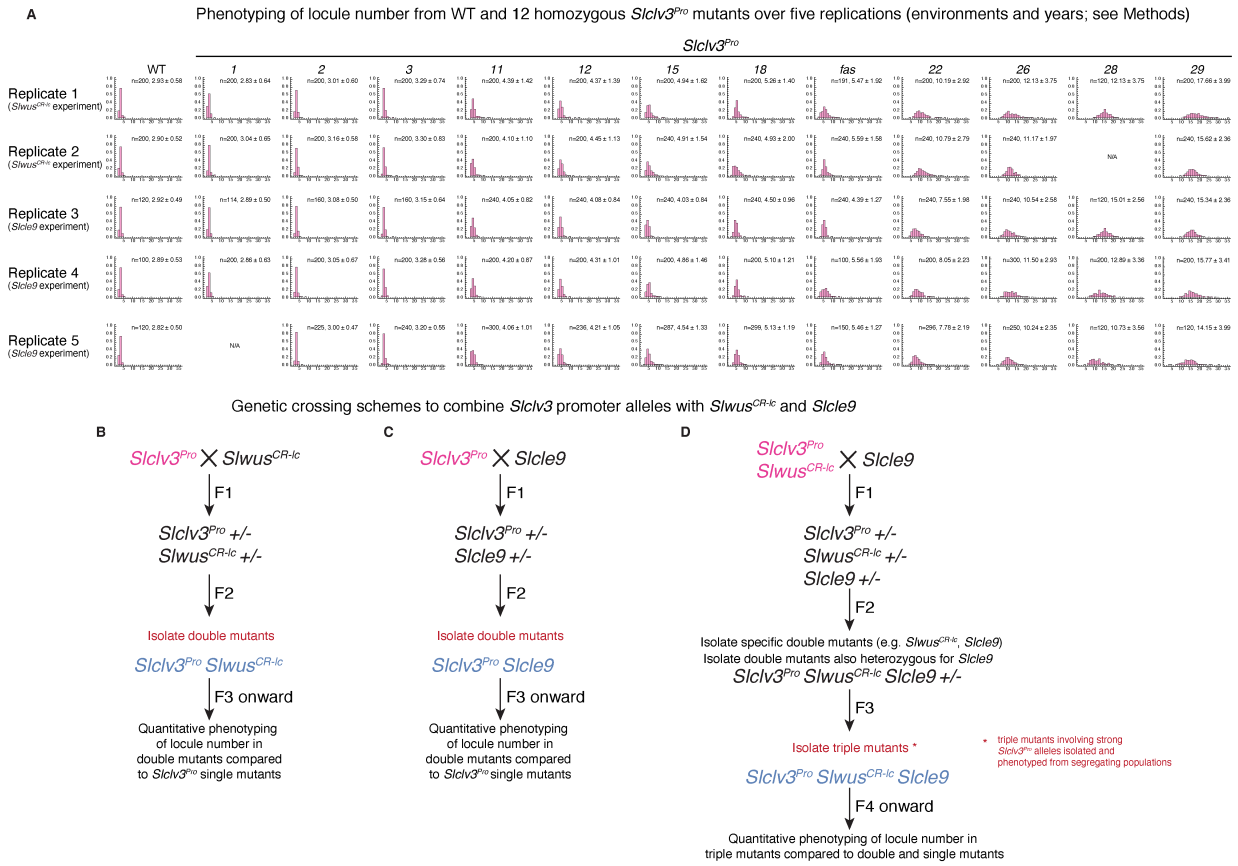

Fig. S1. Genetic schemes used to generate double and triple mutant allele combinations for phenotypic analysis, and reproducibility of phenotypic effects from the *Slclv3^{Pro}* allelic series. (**A**) Histograms from five replicated trials showing the distribution of locule numbers for WT and each homozygous *Slclv3^{Pro}* mutant genotype from different years and environments (Replicate 1- New York, summer 2021; Replicate 2- Florida, fall 2021; Replicate 3- Florida, spring 2021; Replicate 4- New York, summer 2020; Replicate 5- Florida, spring 2020; Supplementary Materials, Growth conditions and phenotyping; table S3). Data demonstrates the consistency of phenotypic effects from each *Slclv3^{Pro}* mutant allele, as well as reproducibility of the inter-allelic relationships. N/A indicates absence of dataset. Top right shows number of fruits (*n*) and mean ±1 standard deviation for each genotype. (**B-D**) Genetic crossing scheme for generating *Slclv3^{Pro} Slwus$^{CR\text{-}lc}$* and *Slclv3^{Pro} Slcle9* double mutant genotypes (B, C respectively), and *Slclv3^{Pro} Slwus$^{CR\text{-}lc}$ Slcle9* triple mutant genotypes (D). All mutant alleles were Cas9 negative and backcrossed at least twice to WT before crossing to other mutant backgrounds (Supplementary Materials, Plant material and genotyping).

Supplementary Figure 2

Fig. S2. Effects of *Slwus*$^{CR\text{-}lc}$ and *Slcle9* on fruit locule number across the *Slclv3*^{Pro} allelic series. (**A**) Histograms of the distribution of locule number for WT and the indicated *Slclv3*^{Pro} single mutants (pink bars) and corresponding *Slclv3*^{Pro} *Slwus*$^{CR\text{-}lc}$ double mutants (light blue bars) in two replicated trials (Replicate 1- New York, summer 2021; Replicate 2- Florida, fall 2021; Supplementary Materials, Growth conditions and phenotyping; table S3). The *Slclv3*$^{Pro\text{-}29}$ allele is a 7.3kb deletion that removes entirety *SlCLV3* coding sequence and its *cis*-regulatory regions. This null allele, has the same effect on locule number as CRISPR-Cas9 generated *Slclv3* coding mutations that cause a frame-shift. Top right indicates number of fruits (*n*) and mean ±1 standard deviation for each genotype. (**B**) Histograms of the distribution of fruit locule number for WT, the indicated *Slclv3*^{Pro} single mutants (pink bars), and the corresponding *Slclv3*^{Pro} *Slcle9* double mutants (light blue bars) in three replicated trials (Replicate 1- Florida, spring 2021; Replicate 2- New York, summer 2020; Replicate 3- Florida, spring 2020; Supplementary Materials, Growth conditions and phenotyping; table S3). Top right indicates number of fruits (*n*) and mean ± 1 standard deviation for each genotype. The *Slclv3*$^{Pro\text{-}29}$ *Slcle9* data presented in Replicate 1 is an aggregation from fruits harvested across multiple field seasons (table S3). (**C**) Histograms of the normalized distributions of fruit locule number of *Slclv3*^{Pro} *Slwus*$^{CR\text{-}lc}$ double mutants (pink bars) and *Slclv3*^{Pro} *Slwus*$^{CR\text{-}lc}$ *Slcle9* triple mutants (light blue bars). Top right indicates number of fruits (*n*) and mean ±1 standard deviation for each genotype. The *Slclv3*$^{Pro\text{-}29}$ null mutant alone and in combination with *Slwus*$^{CR\text{-}lc}$ and *Slcle9* as double mutant sets fewer fruits from flowers compared to other *Slclv3*^{Pro} mutants. Thus, carpel numbers from fully developed flowers were quantified as a supplement to locule numbers (Florida, spring 2022; Supplementary Materials, Growth conditions and phenotyping; table S3).

Supplementatry Figure 3

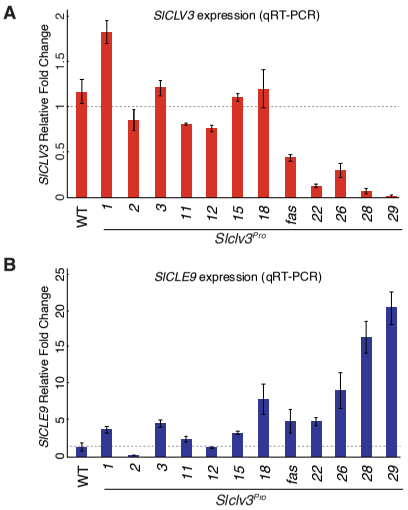

Fig. S3. Expression analysis of *SlCLV3* and *SlCLE9* in reproductive meristem tissue across homozygous mutants of the *Slclv3^{Pro}* allelic series. (**A-B**) qRT-PCR showing expression of *SlCLV3* (A) and *SlCLE9* (B) in WT and the indicated *Slclv3^{Pro}* mutant genotypes. Values are means ± 1 standard error from three biological replicates of pooled reproductive meristems (Supplementary Materials, RNA extraction and Quantitative RT-PCR (qPCR); table S3). Expression is normalized to the control gene *SlUBIQUITIN* and shown as fold change relative to WT.

Captions for Supplementary data

Table S1.
Allelic information for all single, double, and triple mutants used in this study.

Table S2.
Model comparison and supplemental statistical analysis of pairwise and three-way epistasis.

Table S3.
Locule number counts raw data from all seasons and qRT results.

Table S4.
Oligonucleotide primers used in this study.